International Journal of Nanomedicine

Dovepress
open access to scientific and medical research

Open Access Full Text Article

ORIGINAL RESEARCH

The New Nano-Resuscitation Solution (TPP-MR) Attenuated Myocardial Injury in Hemorrhagic Shock Rats by Inhibiting Ferroptosis

Lei Tan[1,2,*], Han She[1,2,*], Yi Wang[1,2,*], Yuanlin Du[1], Jun Zhang[1], Yunxia Du[1], Yinyu Wu[1], Wei Chen[1], Bingqiang Huang[1], Duanyang Long[1], Xiaoyong Peng[2], Qinghui Li[2], Qingxiang Mao[1], Tao Li[2], Yi Hu[1]

[1]Department of Anesthesiology, Daping Hospital, Army Medical University, Chongqing, 400042, People's Republic of China; [2]State Key Laboratory of Trauma, Burns and Combined Injury, Shock and Transfusion Department, Daping Hospital, Army Medical University, Chongqing, 400042, People's Republic of China

*These authors contributed equally to this work

Correspondence: Tao Li; Yi Hu, Email lt200132@163.com; huyi921@sina.com

Background: Hemorrhagic shock was a leading cause of death worldwide, with myocardial injury being a primary affected organ. As commonly used solutions in fluid resuscitation, acetated Ringer's (AR) and Lactate Ringer's solution (LR) were far from perfect for their adverse reactions such as lactic acidosis and electrolyte imbalances. In previous studies, TPP@PAMAM-MR (TPP-MR), a novel nanocrystal resuscitation fluid has been found to protect against myocardial injury in septic rats. However, its role in myocardial injury in rats with hemorrhagic shock and underlying mechanism is unclear.

Methods: The hemorrhagic shock rats and hypoxia-treated cardiomyocytes (H9C2) were utilized to investigate the impact of TPP-MR on cardiac function, mitochondrial function, and lipid peroxidation. The expressions of ferritin-related proteins glutathione peroxidase 4 (GPX4), Acyl CoA Synthase Long Chain Family Member 4 (ACSL4), and Cyclooxygenase-2(COX2) were analyzed through Western blotting to explore the mechanism of TPP-MR on hemorrhagic myocardial injury.

Results: TPP-MR, a novel nanocrystalline resuscitation fluid, was synthesized using TPP@PAMAM@MA as a substitute for L-malic acid. We found that TPP-MR resuscitation significantly reduced myocardial injury reflected by enhancing cardiac output, elevating mean arterial pressure (MAP), and improving perfusion. Moreover, TPP-MR substantially prolonged hemorrhagic shock rats' survival time and survival rate. Further investigations indicated that TPP-MR improved the mitochondrial function of myocardial cells, mitigated the production of oxidative stress agents (ROS) and increased the glutathione (GSH) content. Additionally, TPP-MR inhibited the expression of the ferroptosis-associated GPX4 protein, ACSL4 and COX2, thereby enhancing the antioxidant capacity.

Conclusion: The results showed that TPP-MR had a protective effect on myocardial injury in rats with hemorrhagic shock, and its mechanism might be related to improving the mitochondrial function of myocardial cells and inhibiting the process of ferroptosis.

Keywords: myocardial injury, hemorrhagic shock, mitochondria, ferroptosis

Introduction

Hemorrhagic shock, caused by acute blood loss, was characterized by a decrease in actual circulating blood volume, insufficient tissue perfusion, metabolic disorder, and organ dysfunction.[1] According to the World Health Organization, approximately 1.9 million people worldwide died from hemorrhagic shock in 2016 alone.[2] In the United States, hemorrhagic shock was one of the leading causes of death among people under 46 years old.[3] The heart was the organ most commonly implicated in hemorrhagic shock, and once cardiac dysfunction happened, the prognosis further deteriorated.[4,5] Previous studies reported that the mechanisms of myocardial injury in hemorrhagic shock were mainly related to inflammation, autonomic dysfunction, and apoptosis.[6,7] However, the therapeutic efficacy targeted to these mechanisms was not ideal.

Received: 12 March 2024
Accepted: 21 June 2024
Published: 25 July 2024

Fluid resuscitation was a key emergency treatment for hemorrhagic shock as it could quickly replenish the actual blood volume and improve systemic perfusion.[8] Lactate Ringer's solution (LR) was commonly used in fluid resuscitation. However, extensive use of LR might further increase the high lactate levels caused by tissue hypoxia. With acetate as the source of bicarbonate, Acetated Ringer's solution (AR) could avoid the accumulation of lactic acid. Compared with acetate, malic acid had a longer half-life and thus could continuously produce $HCO3^-$ to maintain the acid-base balance. In addition, as a key intermediate metabolite of the tricarboxylic acid cycle and a major source of mitochondrial ATP. Malic acid has been reported to alleviate myocardial ischemia-reperfusion injury, enhance myocardial contractility, reduce the expression of inflammatory factors, and inhibit apoptosis.[9,10] Nevertheless, rapid infusion of a large amount of fluid often increased the burden on the heart and led to abnormal coagulation, cell edema, and mitochondrial dysfunction, thus limiting the effectiveness of resuscitation.[11] Developing better resuscitation solution was a key strategy to improve hemorrhagic shock. TPP@PAMAM-MR(TPP-MR) was a novel type of nanocrystal resuscitation fluid, exhibiting a stronger targeted capability towards myocardial mitochondria. TPP-MR was synthesized by replacing the L-malic acid in MR with TPP@PAMAM@MA which was a polymer formed by wrapping L-malic acid with a triphenylphosphine material modified with polyamidoamine (PAMAM).[12] Our previous study indicated that TPP-MR significantly protected against myocardial injury in sepsis.[13] However, it remained unclear whether TPP-MR offered protection against myocardial injury in hemorrhagic shock.

Ferroptosis was first coined by Scott J. Dixon et al[14] in 2012. As a programmed iron-dependent cell death form, ferroptosis was found to participate in various pathological and physiological conditions, including septic shock, ischemia-reperfusion injury, and targeted therapy of malignant tumors.[15] Caused by the redox imbalance, ferroptosis was usually accompanied by the accumulated reactive oxygen species (ROS), polyunsaturated fatty acid chains in phospholipids, and iron, resulting in the damage of the integrity of the phospholipid bilayer and the rupture of cell membrane and organelle membrane, ultimately leading to oxidative cell death. Previous studies showed a close relationship between ferroptosis and myocardial dysfunction. Animal experiments conducted by Han She et al[16] found that sepsis led to mitochondrial-related ferroptosis and myocardial injury, which could be alleviated through inhibition of voltage-dependent anion channel 2 (VDAC2) malonylation by a mitochondria targeting nano material. Zeng et al[17] proved that inhibiting ferroptosis by resveratrol through the Sirt1/Nrf2 pathway could alleviate myocardial dysfunction induced by sepsis in rats. However, whether the myocardial dysfunction in hemorrhagic shock rats was related to ferroptosis was unclear.

Therefore, we conducted animal and cell experiments to verify our hypothesis that TPP-MR might have the protective effects on myocardial function in hemorrhagic shock, which was related to ferroptosis.

Materials and Methods

Ethical Approval of the Study Protocol

The study protocol was approved by the Laboratory Animal Welfare and Ethics Committee of Army Medical University (Approval No. AMUWEC20224867). The investigation conformed to the Guide for the Care and Use of Laboratory Animals published by the US National Institutes of Health (8th edition, 2011, National Institutes of Health, Bethesda, Md).

Reagents

Lactate Ringer's solution was purchased from Sichuan Kelun Pharmaceutical (Sichuan, China). Malate Ringer's solution was purchased from B. Braun (Melsungen AG, Germany). Sodium chloride, potassium chloride, calcium chloride, magnesium chloride and sodium acetate were purchased from Macklin Biochemical Co Ltd (Shanghai, China). ATP detection kit was purchased from Cell Biolabs, Inc (San Diego, USA). OCR (mitochondrial respiration detection) kit was purchased from Sigma (St. Louis, Missouri, USA). GPX4 (ab125066) and ACSL4 (ab205199) were purchased from Abcam (Cambridge, MA, USA). β-actin (Cat. BM0627) was purchased from Boster (China). COX2 (12,282) was purchased from Cell Signaling Technology (Danvers, Massachusetts, USA). MitoTracker Deep Red (M22426) and Mito-SOX Red (M36008) were purchased from Invitrogen (Carlsbad, CA, USA). MitoBright-Deep Red (MT12) and Mito-FerroGreen (M489) were purchased from Dojindo (Kyushu, Japan). Lipid Peroxidation kit

(C10445) was purchased from Thermo Scientific (Waltham, MA, America). JC-1 (C2003S), MDA (S0131M), and Glutathione detection kit (S0053) were purchased from Beyotime Biotechnology (Shanghai, China). DAPI (Cat. ab188804) was purchased from Abcam company (USA). Ferrostatin-1 (Cat. #SML0583) was purchased from Sigma-Aldrich (St. Louis, MO). Triphenyl phosphine (TPP)(T84409) and polyamidoamine(PAMAM) (412,449) were purchased from Sigma (St. Louis, Missouri, USA).

Synthesis of TPP@PAMAM@MA

Triphenylphosphine (TPP, 10 mmol) and 6- bromohexanoic acid (10.5 mmol) were dissolved in anhydrous acetonitrile and refluxed for 16 hours under the protection of nitrogen. After the reaction, the product was recrystallized to obtain TPP-COOH. TPP-COOH (2 mmol), N, N'- dicyclohexylcarbodiimide (2.4 mmol), and N-hydroxysuccinimide (NHS, 2.4 mmol) were mixed in 10 mL of anhydrous DMSO and reacted at room temperature for 12 hours. Then PEG(1 mmol) was added and the reaction continued at room temperature for another 12 hours. After that, the reaction solution was transferred to a dialysis bag (molecular weight cut-off 1000), dialyzed with DMSO for 24 hours and deionized water for 48 hours successively. The dialysate was freeze-dried to obtain an intermediate product (TPP-PEG). Subsequently, TPP-PEG(1 mmol), N, N'- dicyclohexylcarbodiimide (1.2 mmol) and N- hydroxysuccinimide (NHS, 1.2 mmol) were mixed in 5 mL of anhydrous DMSO and reacted at room temperature for 24 hours. Polyamide amine (PAMAM, 3mmol) was added and the reaction continued for 24 hours. The reaction solution was transferred to a dialysis bag (molecular weight cut-off 2000), dialyzed with DMSO for 24 hours and deionized water for 48 hours. Freeze-drying the dialysate to obtain an intermediate product (TPP-PEG-PAMAM). Finally, an equal proportion of malic acid and TPP-PEG-PAMAM solution was gently mixed by vortex for 30 seconds, and left it at room temperature for 30 minutes to form TPP-PEG-PAMAM malic acid polymer (TPP@PAMAM@MA). TPP@PAMAM@MA was dissolved in DMSO and characterized by 1HNMR, particle size distribution, zeta potential and electron microscope.

Organ Toxicity and Cytotoxicity Testing of TPP@PAMAM@MA

TPP@PAMAM@MA was dissolved in sterile water to prepare a 10 mg/mL solution. The solution was injected intravenously into rats at a dose of 30 mg/kg. After 24 hours, the tissues of rat heart, liver and kidney were collected for H&E staining. About 5000 cardiomyocytes (H9C2) were cultured in 96-well plates and treated with 1ug/mL solution at 37°C for 15 minutes. Then cell viability was measured by cell counter.

Preparation of TPP-MR

TPP@PAMAM@MA was synthesized by nano-material synthesis technology. MR was prepared in the following proportions: sodium chloride 6.799 g, potassium chloride 0.2984 g, calcium chloride 0.3675 g, magnesium chloride 0.2033 g, sodium acetate 3.266 g, L-malic acid 0.671 g and sodium hydroxide 0.2 g, and the volume was adjusted to 1000 mL with water for injection. In TPP-MR, L-malic acid in MR was replaced by TPP@PAMAM@MA to form a new resuscitation fluid. The drug load and encapsulation rate of TPP-MR was24.27% and 80.09%, respectively.[18] Based on the drug load and peak load rate, TPP-MR was prepared using an equivalent mass of L-malic acid and TPP@PAMAM@MA.

Metabolism Analysis of TPP-MR in vivo

Thirty SD rats were randomly divided into groups for ten time points, each group consisting of 3 rats. TPP-MR was administered intravenously at a dose of 35mL/kg. Blood was collected from the abdominal main vein at 10 minutes, 30 minutes, 1 hour, 2 hours, 4 hours, 8 hours, 24 hours, 36 hours, 48 hours, and 72 hours post-administration, and the rats were euthanized immediately after dissection. The 200uL of plasma was mixed with 400uL of methanol, vortexed for 1 minute, centrifuged at 12000r/min for 10 minutes at 4°C, and the supernatant was collected. The supernatant was then freeze-dried, redissolved in 100uL of methanol, centrifuged at 12,000 r/min for 10 minutes, and 10uL of the ultimate supernatant was used for metabolism analysis by the LC-MS/MS system.

Hemorrhagic Shock Model and Groups

Adult SD rats (weight 200–220 g, provided by the experimental animal center of Daping Hospital of Army Medical University) were anesthetized by intraperitoneal injection of sodium pentobarbital (45 mg/kg). SD rats fasted for 8 hours before the operation but drank water freely. Each animal's right femoral artery and femoral vein were isolated and cannulated with polyethylene tubing (0.9×0.5 mm) for bleeding, monitoring the mean arterial pressure (MAP) and infusion. Blood was withdrawn through the suitable femoral artery catheter to maintain the MAP at 40 mmHg to induce hemorrhagic shock.[19]

A total of 198 SD rats were randomly divided into four groups. The sham group was given an incision without bleeding, and the shock group only received the hemorrhagic shock modeling. At 4 hours after HS surgery, the Fer-1 group was infused with Lactated Ringer's solution (LR, 35mL/kg) and was injected with ferrostatin-1 (Fer-1, ferrostatin-1 0.8mg/kg) in the tail vein at the same time.[20] For the animals in the TPP-MR group, LR was replaced by TPP-MR (35mL/kg) at a constant rate of 2.5mL/h. After the infusion, the blood vessels were ligated, and the incision was sutured. Then, the mean survival time and the survival rate of rats within 24 hours were recorded, and the following experiments were carried out.

Cell Culture and Processing

The H9C2 cardiomyocytes were obtained from the American Type Culture Collection (ATCC, Manassas, VA, United States) and cultured in DMEM supplemented with 10% FBS in a humidified, 5% CO_2/ 95% air atmosphere at 37°C. The cells in this state were the normal group. The cells were treated with hypoxia to simulate the state of hemorrhagic shock in animals for mechanism research. H9C2 cells were seeded in a culture dish for 12 hours and then were placed in a sealed tank at 37°C for hypoxia treatment. The cells underwent hypoxia process involved first introducing anoxic gas (95% N2 and 5% CO2) for 15 minutes, then closing the vent valve for 10 minutes, and reopening the vent valve to introduce anoxic gas again. This hypoxia process was repeated four times until the oxygen concentration in the sealed tank fell below 0.2%. The tank was then sealed for 4 hours. Hypoxic cells were randomly divided into 3 groups, including the hypoxia group which only received hypoxia treatment, Fer-1 group and TPP-MR group which received Fer-1 (5uM)[21]+1% volume of LR (1% of the volume of the culture medium in the culture dish) or only 1% volume of TPP-MR solution (1% of the volume of the culture medium in the culture dish) during the tank sealed for 4 h, respectively.

Cardiac Output Measurement and Oxygen Supply and Consumption Testing

In each group, rats underwent catheterization of the jugular vein, with the catheter opening positioned at the right heart atrium. A thermodilution catheter was inserted into the carotid artery up to the proximal end of the aorta, with the depth adjusted until the catheter showed noticeable pulsation with the heartbeat and connected to a cardiac output measuring device. A temperature probe was placed in 0°C ice-salt water until the temperature stabilized. Then, 0.3 mL of ice-salt water was rapidly injected through the venous catheter, and the cardiac output (CO) and heart rate (HR) of each group of rats were measured using a Cardiomax III (USA). The cardiac index [CI = CO ÷ S, body surface area: $S = K \times W^{(2/3)}$ (cm^2), where K = 9.1; W: body weight (g)] and stroke index (SI = CI ÷ HR) were calculated using these measurements. After that, arterial and venous blood samples were collected from the femoral artery and vein for blood gas analysis: oxygen tension (pO2), hemoglobin (Hb), arterial oxygen saturation (SaO_2), and venous oxygen saturation (SvO_2). Tissue oxygen delivery ($DO_2 = CI \times 13.4 \times Hb \times SaO_2$) and consumption [$VO_2 = CI \times 13.4 \times Hb \times (SaO_2 - SvO_2)$] were calculated.

Echocardiographic Assessment in Rats

Echocardiographic assessment was conducted using a Vevo2100 small animal echocardiography system and a corresponding MS-400 high-frequency probe. Images of the left ventricular short-axis view were captured in rats under 0.4% pentobarbital sodium intraperitoneal anesthesia. Left ventricular posterior wall thickness in diastole (LVPWTD), left ventricular posterior wall thickness in systole (LVPWTs), left ventricular end-diastolic diameter (LVEDD), left ventricular end-systolic diameter (LVESD), left ventricular mass, left ventricular ejection fraction (LVEF), and left ventricular short-axis fractional shortening (FS) were calculated.

Mitochondrial Respiration Measurement

In an XF24 cell culture plate, excluding background correction wells, each well was inoculated with 100 μL of cardiomyocyte suspension at a density of 10K cells/100μL/well. The cells were allowed to adhere for 1 hour before adding 150 μL of high-glucose culture medium to each well. After various treatments, the cell culture plate was incubated for 12 hours in a 37°C CO_2 incubator. Meanwhile, 1 mL XF Calibrant was added to each well of a hydration plate. The entire probe plate assembly was hydrated overnight in a 37°C non-CO_2 incubator. On the day of the experiment, each well of the cardiomyocyte culture plate was washed twice with assay medium, ensuring 500 mL of assay medium in each well, and then incubated in a 37°C non-CO_2 incubator for 60 minutes before testing with the XF Cell Mito Stress Test Kit.

Mitochondrial Membrane Potential Measurement

Cardiomyocytes were seeded onto confocal culture dishes and treated according to group protocols once cell coverage reached about 70%. Added ultrapure water to 50ul of 200x JC-1 to reach a total volume of 8 mL, mixed well, and then added 2 mL of staining buffer (5x) to mix to prepare the JC-1 staining working solution. Each culture dish was incubated with 0.5 mL of JC-1 working solution in a 37°C incubator for 20 minutes, then washed twice with JC-1 staining buffer (1x) and finally replaced with cell culture medium before observing JC-1 expression under a laser confocal microscope. Normal cells should show red fluorescence due to intact mitochondrial membrane potential, while cells with lost membrane potential should exhibit green fluorescence.

Mitochondrial Reactive Oxygen Species Detection

Cardiomyocytes reached to 70% confluency in confocal culture dishes were treated with ROS detection working solution at a final concentration of 10 umol/L and incubated in a 37°C incubator for 30 minutes. The culture dishes were gently shaken every 5 minutes to ensure full contact between the probe and cells. After incubation, cells were washed three times with serum-free culture medium, replaced with pre-warmed fresh cell culture medium at 37°C, and observed under a laser confocal microscope.

Confocal Microscopy Observation of Mitochondrial Morphology

Cardiomyocytes were seeded in confocal culture dishes and treated according to group protocols for 4 hours. Then cells were washed with 37°C PBS and incubated with pre-prepared Mitro Tracker live cell mitochondrial dye (1:10,000) at 37°C for 30 minutes before washing three times with 37°C PBS. Finally, 1 mL of 37°C serum-free culture medium was added to the culture dish, and mitochondrial morphology in cardiomyocytes was observed using a confocal microscope.

Cardiomyocyte Ferrous Ion Detection

Cardiomyocytes were seeded in culture dishes and treated according to group protocols for 30 minutes in a CO_2 incubator before adding 5 μmol/L Mito-FerroGreen and 200 nmol/L MitoBright Deep Red mitochondrial staining probe. Then 100 μmol/L ammonium iron (II) sulfate was added to the cell culture dishes, thoroughly mixed. After 1 hour, the cardiomyocyte ferrous was observed by fluorescence.

Lipid Peroxidation Detection in Cardiomyocytes

Cardiomyocytes were seeded in culture dishes and treated according to group protocols before adding Image iT® lipid peroxidation reagent to achieve a final concentration of 10μM. The cells were then incubated at 37°C for 30 minutes, washed three times with PBS, and the culture medium was replaced with 1 mL of serum-free one pre-warmed at 37°C. Finally, lipid peroxidation was observed using a confocal microscope.

Statistical Analysis

Statistical analysis was performed using SPSS 20.0 (SPSS Inc., Chicago, IL, USA). Data were presented as mean ± standard deviation. Independent sample *t*-tests were used to analyze differences between two groups. One-way analysis

of variance (ANOVA) and post-hoc tests (S-N-K/LSD) were used for multiple group comparisons. P-values less than 0.05 were considered statistically significant.

Results

Characterization and Toxicity of TPP@PAMAM@MA

TPP@PAMAM@MA was verified by mass spectrometry and NMR. Hydrogen spectrum measurement showed malic acid-CH2-1H NMR characteristics at δ2.01 and δ2.24. PAMAM-COOR 1H NMR characteristics were at δ2.01–2.58. TTP-COOH 1H NMR characteristics were at 7.32–7.58 (Ar-H) (Figure 1A). PEG 1H NMR characteristics were at δ2.14–2.21 (-NHCH2CH2-) (Figure 1B). Electron microscope photos showed that TPP@PAMAM@MA was spherical with regular particles (Figure 1C). The synthesized TPP@PAMAM@MA had a potential of (−5.7±0.6) mV, with an average particle size of (122.3±0.8) nm (Figure 1D and E). The -CH2- peak appeared at 2888.74 cm^{-1}, characteristic of methylene. Additionally, the key active carboxyl group peak of TPP@PAMAM@MA appeared at 1115.02 cm^{-1}. The results indicated that the characteristic functional groups of TPP@PAMAM@MA had characteristic absorption peaks (Figure 1F). HE staining results indicated that TPP@PAMAM@MA did not disperse in the liver, kidney, and heart after administration, suggesting the safety of TPP@PAMAM@MA for in vivo use, with pathological scoring conducted as per the mentioned method[22](Figure 1G and Supplementary Figure 1). In vitro experiments were also conducted to assess the toxicity of TPP@PAMAM@MA to cardiomyocytes. CCK-8 analysis showed that TPP@PAMAM@MA did not affect the survival rate of cardioH9C2 cells (Figure 1H). TPP@PAMAM@MA was formulated into a clear and transparent TPP-MR with MR's component ratio, meeting the pH and osmotic pressure requirements for infusion (Figure 1I). LC-MS/MS system analysis showed that the peak concentration (Cmax), the elimination phase half-life (HL_Lambda_z), and the apparent distribution volume (Vz_F_obs) of TPP-MR was 472.1±16.2ng/mL, 10.1±1.1h, and 6722.5±1482.1mL/kg, respectively. (Figure 1J).

TPP-MR Improved Cardiac Function and Survival Time in Rats with Hemorrhagic Shock

Cardiac function was evaluated using echocardiography, showing a significant decrease in LVEF in rats with hemorrhagic shock. After TPP-MR infusion, LVEF significantly improved, with an increase rate of 27.2% compared to the shock group (Figure 2A and B). Additionally, hemorrhagic shock caused significant reductions in cardiac output (CO), cardiac index (CI), and stroke index (SI), which were improved by TPP-MR infusion with increase rates of 44.5%,52.0%, and 26.1%, respectively (Figure 2C–E). MAP dropped from around 114 mmHg in sham rats to 45 mmHg in rats with hemorrhagic shock, which was increased by 89.8% after TPP-MR infusion (Figure 2F). The HE staining of heart pathology slice showed that in sham myocardial tissue, myocardial fibers were arranged orderly and interstitial tissue was sparse. In shock group, myocardial cells exhibited obvious swelling, with vacuole formation, disordered myocardial fiber arrangement, and expanded interstitial space. In the TPP-MR group, interstitial edema of myocardial cells was significantly reduced, interstitial space narrowed, and disordered arrangement of myocardial fibers notably restored, with pathological scoring conducted as per previous studies (Figure 2G and H). Compared to the shock group, cardiac troponin T (cTnT) and lactate dehydrogenase (LDH) in the TPP-MR group significantly decreased, indicating significant improvement in myocardial injury (Figure 2I and J). Oxygen supply and consumption significantly decreased in rats with hemorrhagic shock, which was significantly increased after TPP-MR infusion (Figure 2K). No rats in the shock group survived beyond 12 hours, while survival time in the TPP-MR group was significantly extended to 18.6±5.4 hours, with a 24-hour survival rate of 31.3% (Figure 2L). These results indicated that TPP-MR significantly improved cardiac function in rats with hemorrhagic shock by reducing myocardial injury, increasing cardiac output, improving perfusion, and thereby extending survival time.

TPP-MR Improved Mitochondrial Function in Cardiomyocytes of Rats with Hemorrhagic Shock

To explore whether TPP-MR improved mitochondrial function of cardiomyocytes after hemorrhagic shock, we used hypoxia-treated cardiomyocytes and incubated them with TPP-MR to simulate the rat shock model. Mitochondrial ATP

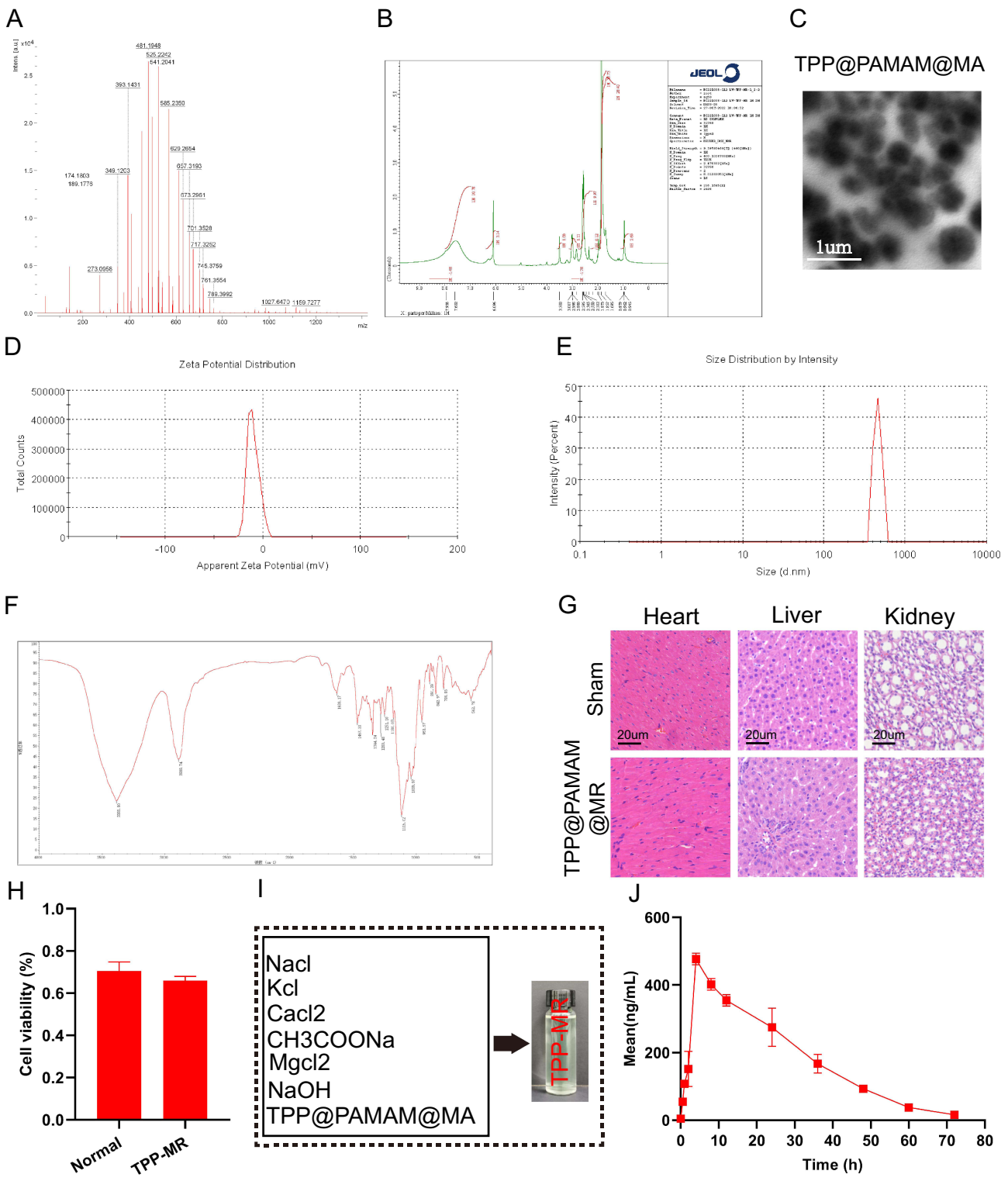

Figure 1 Characterization of TPP@PAMAM@MA. (**A**) TPP@PAMAM@MA mass spectrometry. (**B**) TPP@PAMAM@MA NMR determination. **(C)** The size of TPP@PAMAM@MA was observed under the electron microscope (bar, 1um). (**D**) Potential of TPP@PAMAM@MA. (**E**) Size determination of TPP@PAMAM@MA particle. (**F**) Infrared spectroscopy of TPP-MR. (**G**) HE stains of heart, liver, and kidney after TPP@PAMAM@MA treatment in rats(n=6/group). (**H**) Effect of TPP@PAMAM@MA on the cell viability of H9C2 cells (3 independent experiments). (**I** and **J**) Preparation and pharmacokinetics of TPP-MR.

production and Oxygen Consumption Rate (OCR) were observed by using Agilent hippocampus XF technology. Results showed that TPP-MR treatment improved the reduction of ATP production and OCR of cardiomyocytes caused by hypoxia (Figure 3A–C). Confocal microscopy was used to observe mitochondrial morphology changes. Mitochondria in

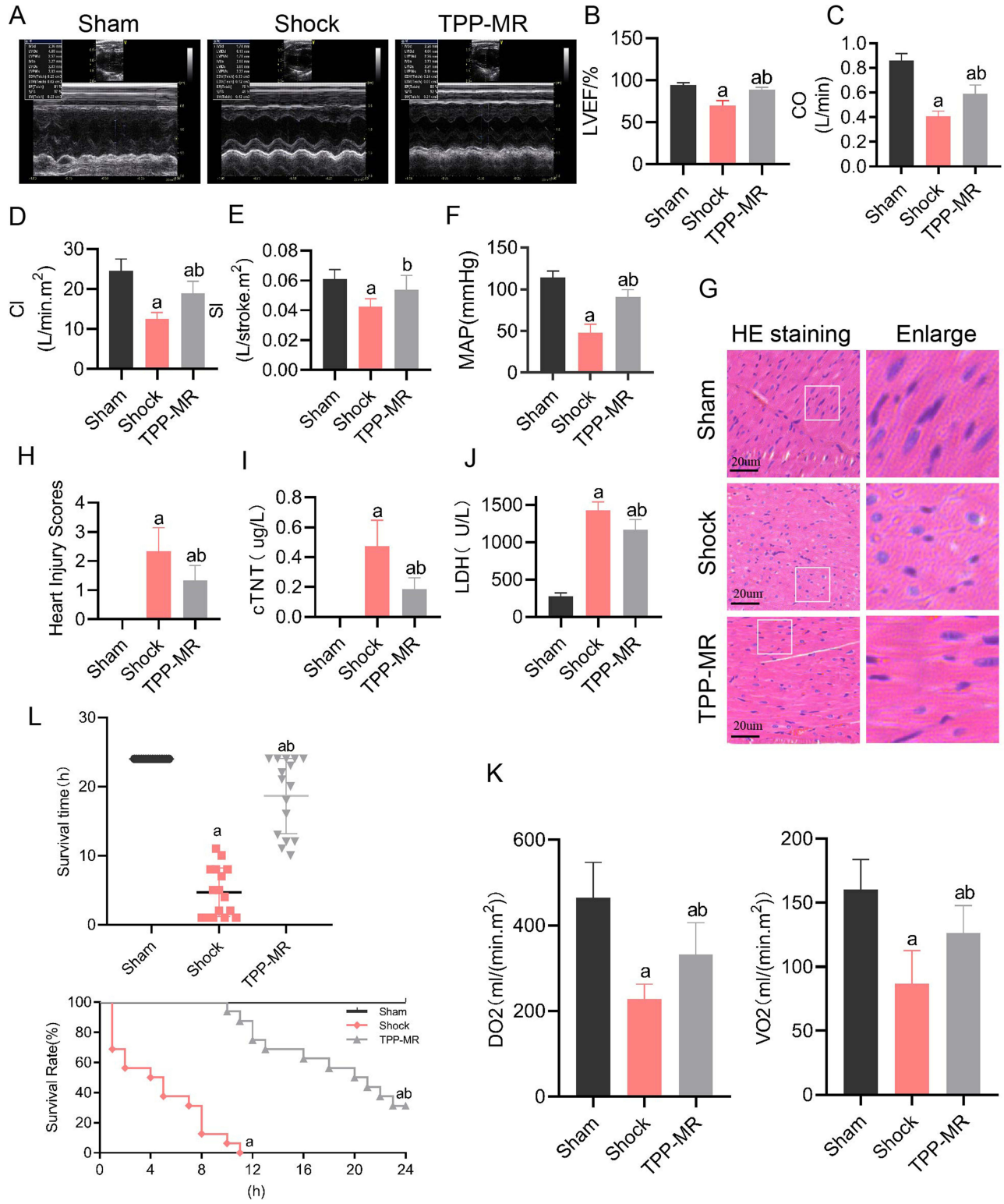

Figure 2 Effects of TPP-MR on cardiac function in hemorrhagic shock rats. Cardiac function including (**A**) echocardiograms (n=6/group), (**B**) LVEF (n=6/group), (**C**) cardiac output (n=8/group), (**D**) cardiac index(n=8/group) and (**E**) stroke index (n=8/group) were measured 2 hours after resuscitation treatment. (**F**) Mean arterial pressure measurement of the hemorrhagic shock rats (n=8/group). (**G** and **H**) HE stains of cardiac pathological sections and heart injury scores (bar, 20um, n=8/group). The expressions of (**I**) cardiac troponin T and (**J**) lactate dehydrogenase in venous blood (n=8/group). (**K**) Detection of oxygen supply and consumption of the hemorrhagic shock rats (n=8/group). (**L**) Survival rate and survival time were observed in different groups (n=16/group). [a]P<0.05 compared with the sham group, [b]P<0.05 compared with the shock group.

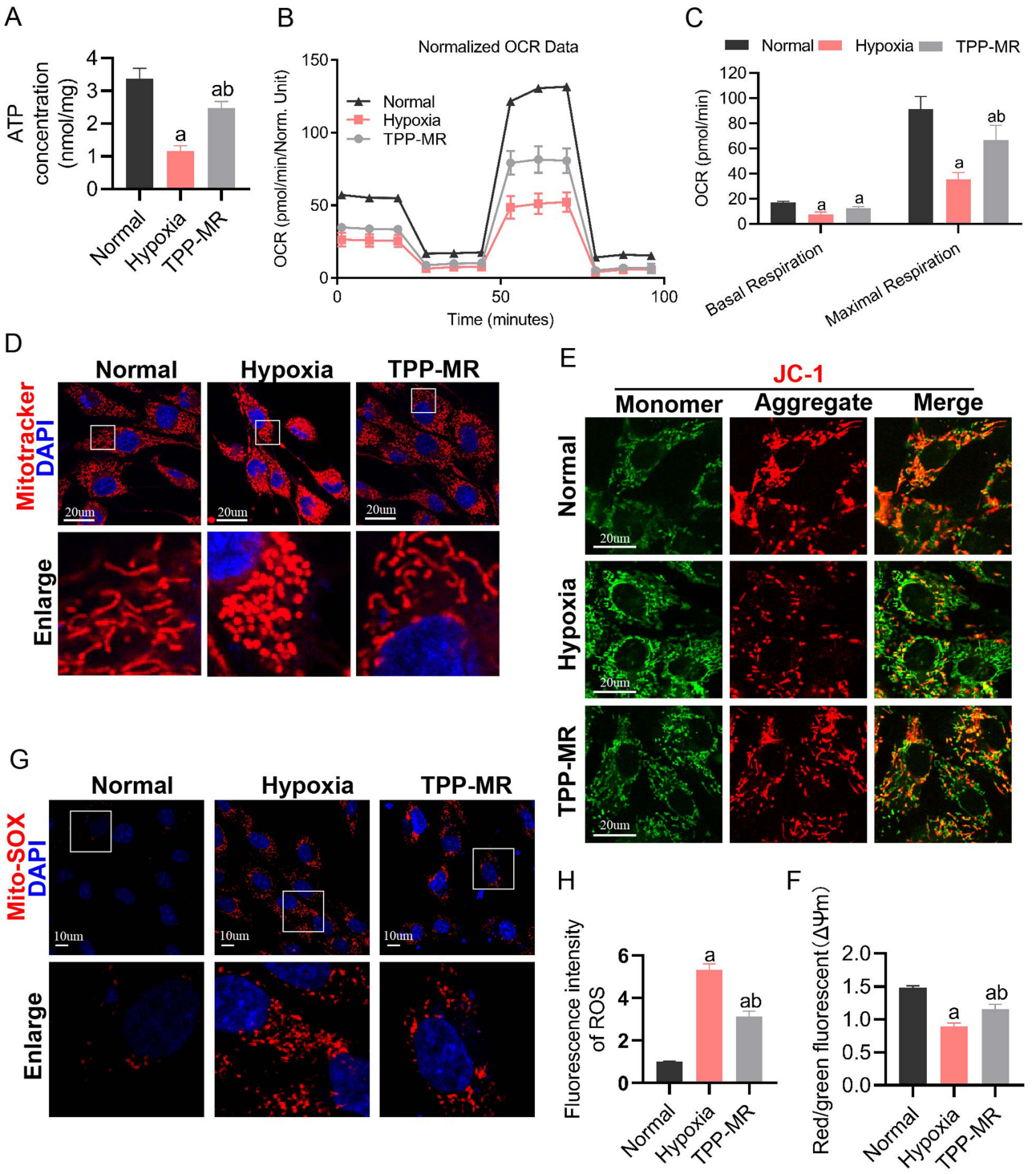

Figure 3 Mitochondrial function of cardiomyocytes hemorrhagic shock. (**A**) Changes in the ATP level (3 independent experiments). (**B** and **C**) Mitochondrial maximum respiratory rate assay in H9C2 (3 independent experiments). (**D**) Representative images of mitochondrial morphology of H9C2 cells (bar, 20um, 3 independent experiments). (**E**) The mitochondrial membrane potential of H9C2 was observed by confocal microscopy (bar, 20um, 3 independent experiments). (**F**) Red/green fluorescent (Δψm) quantitative analysis in H9C2. (**G**) Representative confocal images of MITO-SOX (bar, 10um, 3 independent experiments). (**H**) ROS fluorescence quantitative analysis in H9C2. [a]P<0.05 compared with the normal group, [b]P<0.05 compared with the hypoxia group.

normal cardiomyocytes were distributed as continuous long columns. After hypoxia treatment, most mitochondria in cardiomyocytes undergo morphological changes, presenting as dots or spheres, with a significant increase in the number of mitochondria. TPP-MR incubation restored mitochondrial morphology and significantly reduced the number of

mitochondria (Figure 3D). Further observation of mitochondrial membrane potential and ROS levels in each group showed that after hypoxia treatment, mitochondrial membrane potential in cardiomyocytes significantly decreased and ROS fluorescence intensity significantly increased. TPP-MR was able to counteract the reduction in mitochondrial membrane potential and the increase in ROS fluorescence intensity induced by hypoxia, indicating that TPP-MR infusion could alleviate the damage to mitochondrial function in cardiomyocytes induced by hypoxia (Figure 3E–H).

Hemorrhagic Shock-Induced Myocardial Injury is Associated with Ferroptosis

Reduced glutathione (GSH) and oxidized glutathione (GSSG) played important roles in ferroptosis, while GSH, under the action of GPX4, reduced cell polyunsaturated fatty acid phospholipid hydroperoxides (PUFA-PL-OOHs) to non-lethal PUFA phospholipid alcohols (PUFA-PL-OHs), thereby countering cell ferroptosis. To explore whether myocardial injury in rats with hemorrhagic shock was related to ferroptosis, GSH and GSSG levels in myocardial tissues were measured. Results showed that compared to sham rats, GSH levels decreased, GSSG levels increased, and the GSH/GSSG ratio decreased in the shock group. In contrast, the Fer-1 group showed significantly higher GSH levels, reduced GSSG levels, and an increased GSH/GSSG ratio compared to the shock group (Figure 4A–C). Additionally, lipid peroxidation product MDA level in myocardial tissues significantly increased in the shock group compared to the sham group, which was markedly reduced in the Fer-1 group (Figure 4D). At the cellular level, post-hypoxia Fe^{2+} and lipid peroxidation levels significantly increased compared to the normal group, while Fer-1 notably ameliorated these trends (Figure 4E and F). Western blot results showed that hypoxia significantly increased the expression of ferroptosis-related proteins ACSL4 and COX2, but decreased the GPX4 expression in cardiomyocytes. Compared to the hypoxia group, the Fer-1 group showed a significant decrease in ACSL4 and COX2 expression by 21.3% and 20.0%, respectively, and an increase in GPX4 expression by 15.2% (Figure 4G–J).

Echocardiographic assessment of cardiac function revealed a significant reduction in LVEF in rats with hemorrhagic shock, which was noticeably improved after using the ferroptosis inhibitor Fer-1 (Figure 5A and B). Additionally, hemorrhagic shock caused significant reductions in CO, CI, and SI, which were all significantly improved in the Fer-1 group (Figure 5C–E). MAP also recovered noticeably in hemorrhagic shock rats after using Fer-1 (Figure 5F). HE staining of heart pathology slice showed that interstitial edema of myocardial cells was significantly reduced and the disordered myocardial fiber was restored in the Fer-1 group, with pathological scoring ameliorated (Figure 5G and H). Oxygen supply and consumption were significantly reduced in hemorrhagic shock rats, which were improved after Fer-1 use (Figure 5I). Besides, the ATP production in the Fer-1 group also significantly increased compared to that in the hypoxia group (Figure 5J). At the cellular level, mitochondrial ATP production and OCR were also measured. Results showed that OCR in cardiomyocytes was significantly reduced under hypoxic conditions but noticeably improved after adding the ferroptosis inhibitor Fer-1 (Figure 5K). No rats in the shock group survived beyond 12 hours. In the Fer-1 group, survival time was extended to 10.3±7.7 hours, with a 24-hour survival rate of 4.2% (Figure 5L).

TPP-MR Significantly Inhibits Ferroptosis

Preliminary animal experiments indicated that TPP-MR significantly improved cardiac function in rats with hemorrhagic shock, and myocardial injury in these rats was closely associated with ferroptosis. Western blot results showed that TPP-MR more significantly inhibited ferroptosis compared to the Fer-1 group, further reducing the expression of ferroptosis-related proteins ACSL4 and COX2 by 32.2% and 15.2%, respectively, but slightly increasing the expression of GPX4 by 6.3% in cardiomyocytes after hypoxia stimulation (Figure 6A–D). Similarly, the Fe^{2+} and lipid peroxidation levels further decreased in the TPP-MR group compared to the Fer-1 group (Figure 6E–H). These results suggested that TPP-MR could reduce ROS to inhibit ferroptosis, improve myocardial mitochondrial function, alleviate myocardial injury, enhance cardiac output, improve perfusion, and thereby extend survival time.

Discussion

In this study, we synthesized TPP-MR, a new nano-resuscitation solution for hemorrhagic shock. Our findings demonstrated that TPP-MR protected cardiac function in rats with hemorrhagic shock by improving mitochondrial function and inhibiting cellular ferroptosis. The mechanism might involve the delivery of exogenous malic acid to myocardial cells by

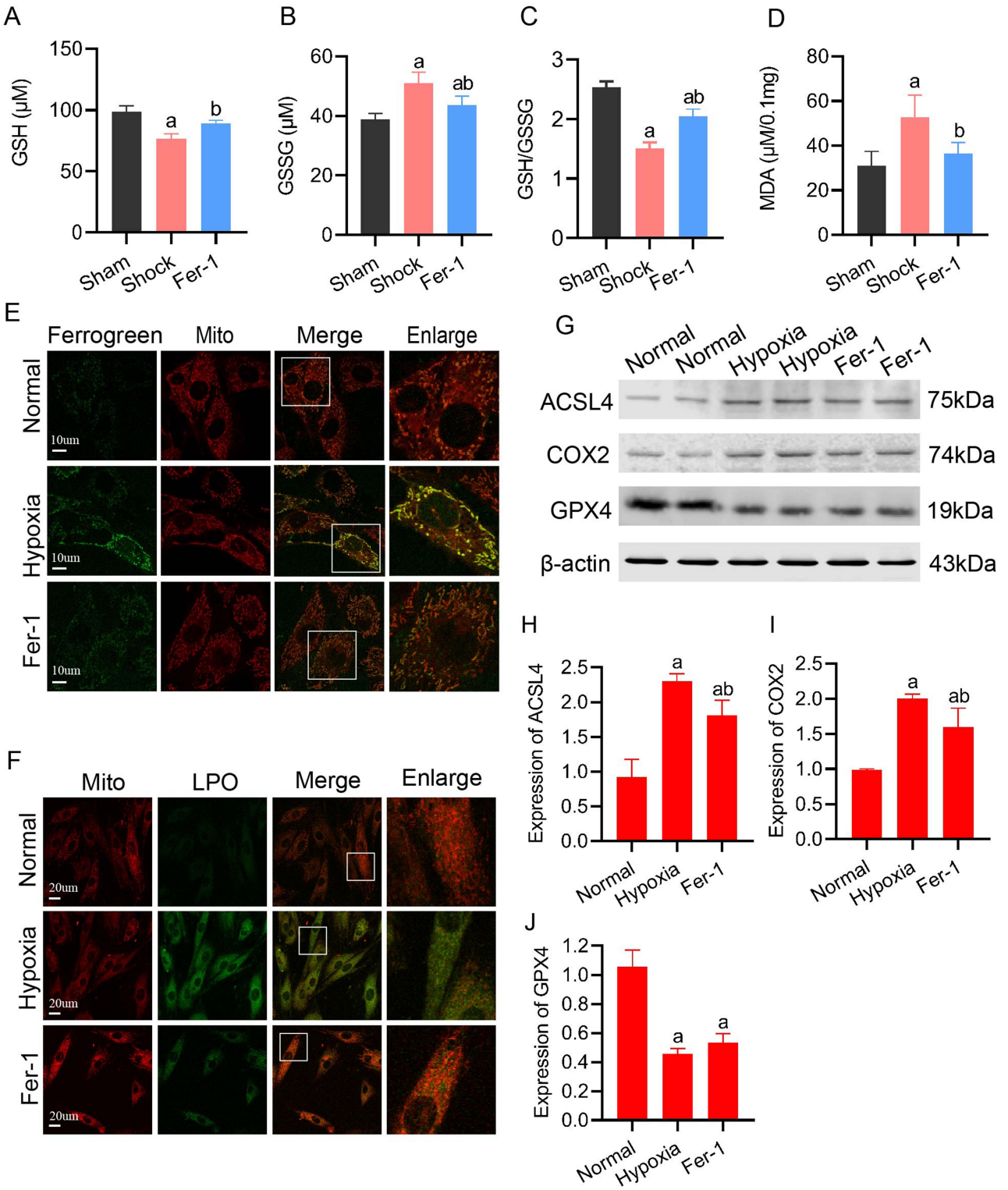

Figure 4 Hemorrhagic shock and ferroptosis. (**A**–**D**) Effects of Hemorrhagic shock on the level of GSH, GSSG, GSH/GSSG and MDA (n=6/group). (**E**) Representative images of H9C2 cells after treatment with MitoBright-Deep Red and Mito-FerroGreen (bar, 10um, 3 independent experiments). (**F**) Representative images of H9C2 cells treated with LPO (bars, 10um, 3 independent experiments). (**G**–**J**)The effect of TPP-MR on the expression of ACSL4, COX2 and GPX4 proteins (3 independent experiments). [a]P<0.05 compared with the sham or normal group, [b]P<0.05 compared with the shock or hypoxia group.

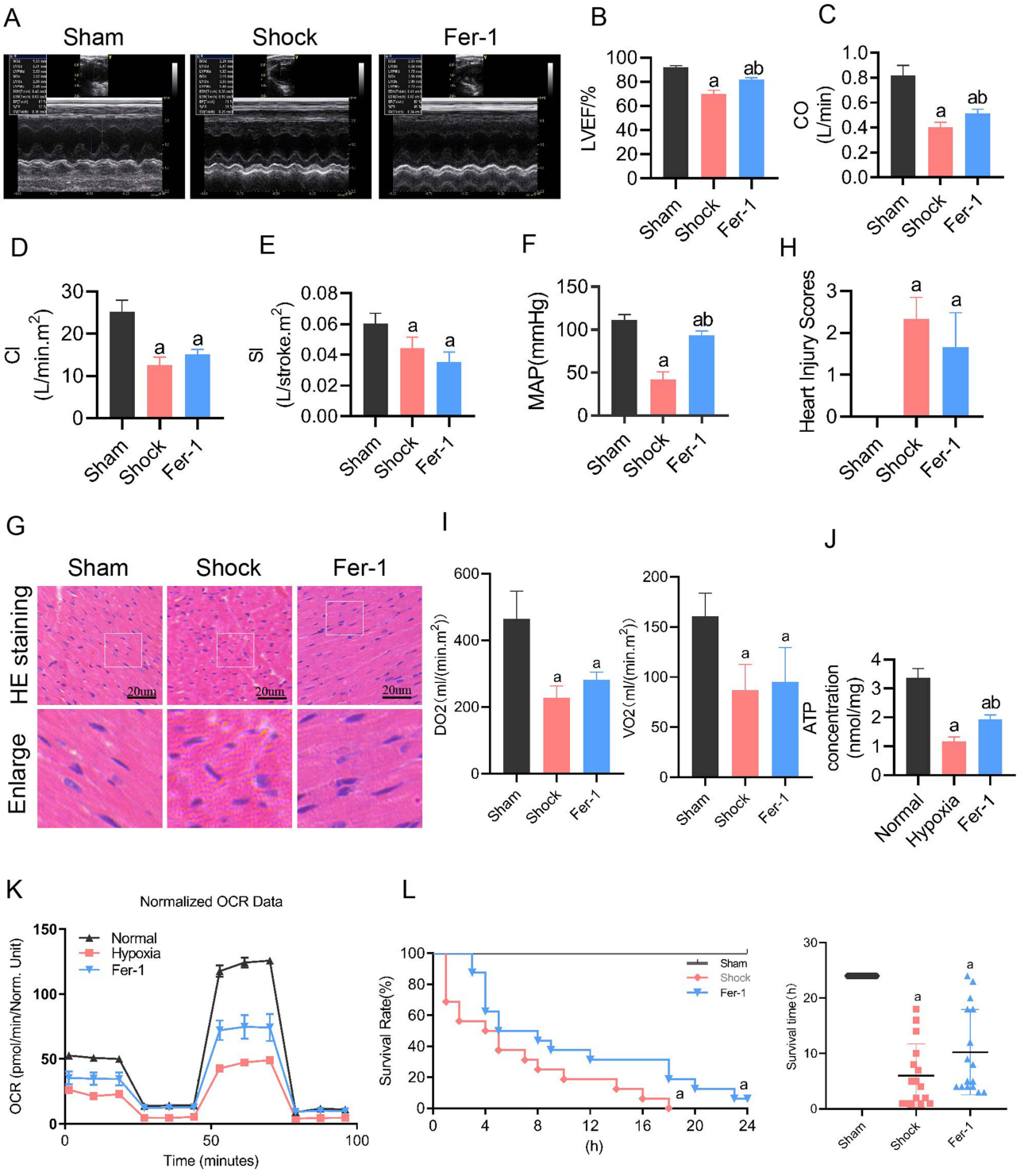

Figure 5 Effects of Fer-1 on myocardial injury in Hemorrhagic shock. Cardiac function including (**A**) echocardiograms (n=6/group), (**B**) LVEF (n=6/group), (**C**) cardiac output (n=8/group), (**D**)cardiac index(n=8/group) and (**E**) stroke index (n=8/group) were measured 2 hours after resuscitation treatment. (**F**) Mean arterial pressure measurement of the hemorrhagic shock rats (n=8/group). (**G**) HE stains of cardiac tissue and (**H**) heart injury score (bar, 20um, n=6/group). (**I**) Detection of oxygen supply and consumption of the hemorrhagic shock rats (n=8/group). (**J**) Changes in the ATP level (3 independent experiments). (**K**) Mitochondrial maximum respiratory rate assay in H9C2 (3 independent experiments). (**L**) The effects of Fer-1 on survival rate and survival time of hemorrhagic shock rats (n=8/group). [a]P<0.05 compared with the sham or normal group, [b]P<0.05 compared with the hemorrhagic shock or hypoxia group.

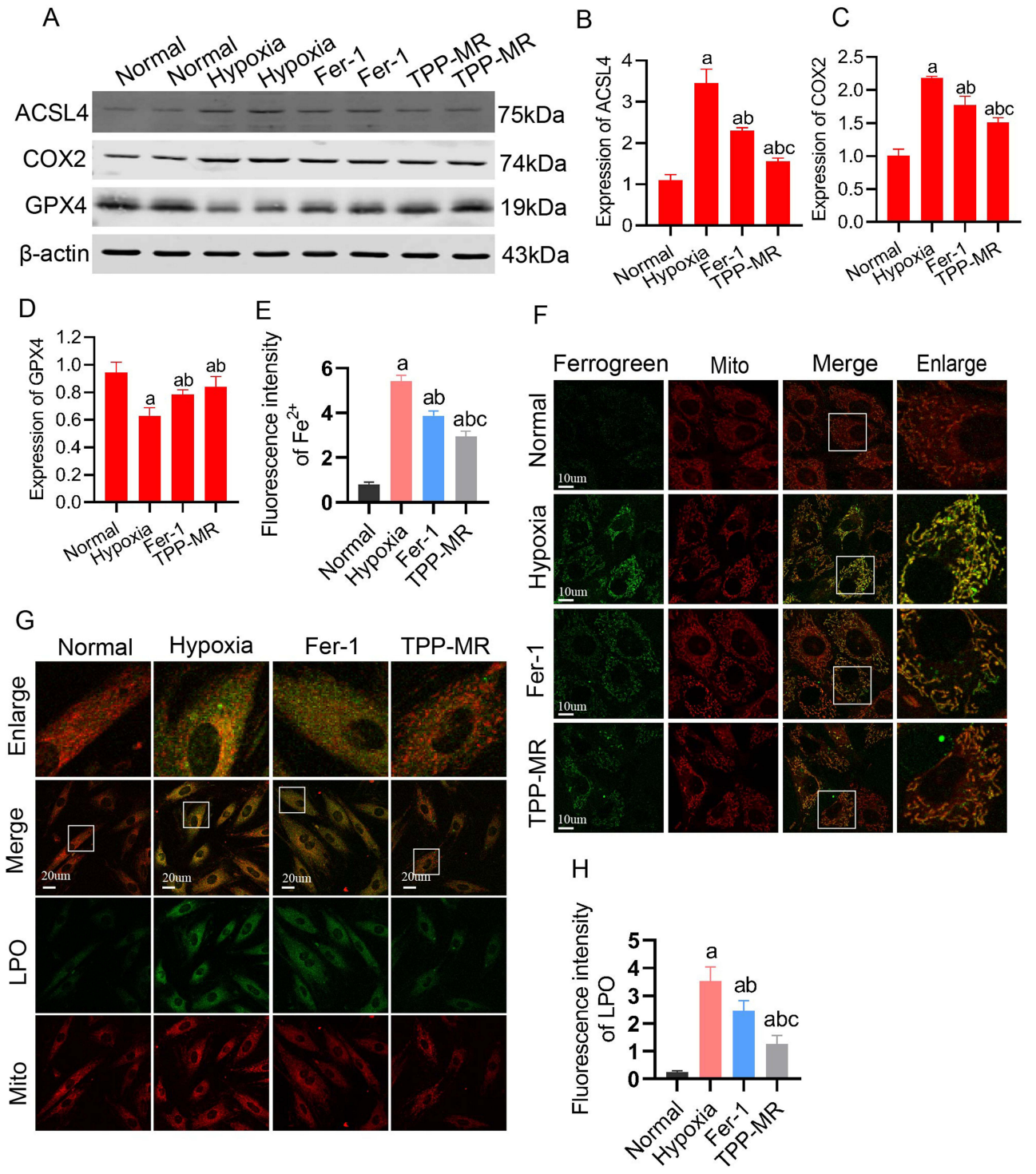

Figure 6 Effect of TPP-MR on H9C2 cells ferroptosis. (**A–D**) The effect of TPP-MR on the expression of ACSL4, COX2 and GPX4 proteins (3 independent experiments). (**E** and **F**) Representative images of H9C2 cells after treatment with MitoBright-Deep Red and Mito-FerroGreen(bar, 10um, 3 independent experiments). (**G** and **H**) Representative images of H9C2 cells treated with LPO (bars, 10um, 3 independent experiments). [a]P<0.05 compared with the sham or normal group, [b]P<0.05 compared with the hypoxia group, [c]P<0.05 compared with the Fer-1 group.

the nanomaterial targeting myocardial mitochondria present in TPP-MR. Malic acid, through the malate-aspartate shuttle, enhanced intracellular ATP production, improved electron transport chain efficiency, and thus improved mitochondrial function. Additionally, TPP-MR reduced mitochondrial ROS production by upregulating GPX4, converting cell phospholipid hydroperoxides (PLOOH) to non-lethal phospholipid alcohols (PLOH), thereby inhibiting cellular ferroptosis. It

also downregulated ACSL4 and COX2, inhibiting the production of PLOOH in cells and thus further preventing ferroptosis (Figure 7).

Hemorrhagic shock was a common critical condition in clinical settings and a major cause of early death in trauma cases.[2] Cardiac dysfunction was one of the most severe complications of hemorrhagic shock and the key factor leading to poor prognosis.[23] Myocardial injury in hemorrhagic shock mainly manifested as reduced myocardial contractility, leading to insufficient systemic blood perfusion and multi-organ dysfunction.[24] Energy supply was crucial for myocardial

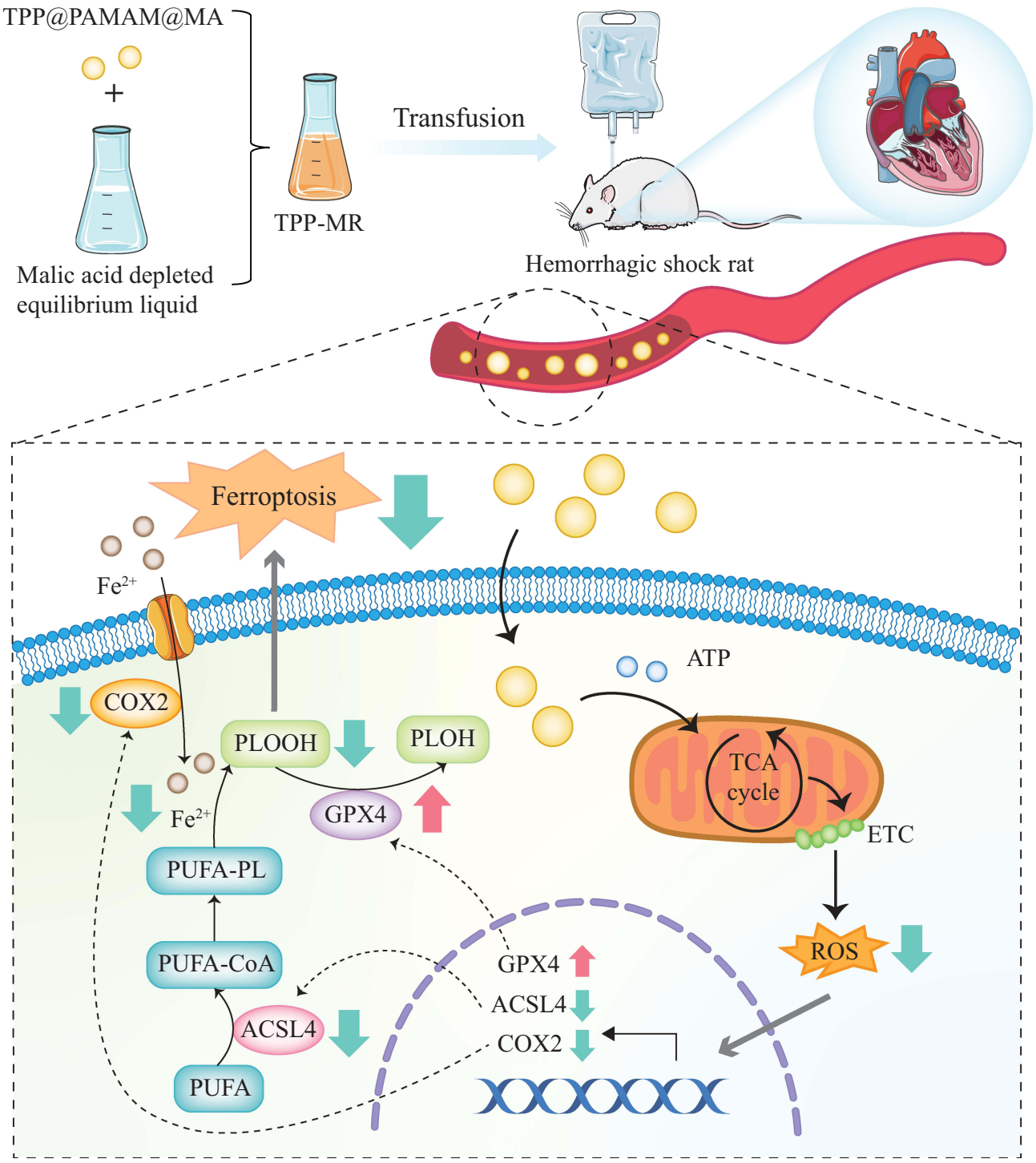

Figure 7 Mechanism of TPP-MR Inhibiting the Ferroptosis. The protective mechanism of TPP-MR on myocardial injury in hemorrhagic shock rats.

contractility. In healthy adult hearts, 70% of energy came from fatty acid β-oxidation, with only 10–30% from glucose metabolism and the rest from lactate, ketone bodies, and amino acid metabolism.[25] Post-hemorrhagic shock, the metabolism of myocardial cell significantly changed, characterized by reduced fatty acid β-oxidation and enhanced glycolysis, leading to a significant reduction in ATP synthesis, and potentially contributing to cardiac dysfunction. Mitochondria, indispensable for regular myocardial cell activity and energy production, undergo various alterations during hemorrhagic shock-induced myocardial injury, including inner membrane damage, permeability changes, membrane potential alterations, and swelling. These changes led to the uncoupling of oxidative phosphorylation, with accompanying calcium ion and cytochrome c efflux, causing a series of mitochondrial dysfunctions, including oxidative phosphorylation damage, decreased kinase activity, and oxidative damage.[26] Therefore, improving mitochondrial function was vital in myocardial injury after hemorrhagic shock.

Fluid resuscitation was the first-line treatment for hemorrhagic shock. Wang et al[27] found that bicarbonate Ringer's solution (BRS) maintained typical glycocalyx structure and mitigated inflammation, maintaining mean arterial pressure in rats with hemorrhagic shock. Zhao et al[28] discovered that HES (130/0.4) protected against endothelial injury in hemorrhagic shock rats by downregulating heparanase, hyaluronidase, and neuraminidase expression. Malate Ringer's (L-malate acetic acid-balanced fluid) was a novel resuscitation fluid containing the indispensable intermediate metabolite L-malate (330mg/500mL). L-malate, via the malate-aspartate shuttle, entered the mitochondrial matrix through the oxaloacetate malate carrier (OMC) channel and was converted to NADH under malate dehydrogenase. NADH reduced oxaloacetate to malate, which penetrated the matrix through the OMC on the mitochondrial inner membrane, regenerating oxaloacetate and NADH. NADH entered the electron respiratory chain to produce ATP. At the same time, matrix-generated oxaloacetate converted to aspartate under the action of glutamate oxaloacetate transaminase, which was then transported out of the matrix by the aspartate glutamate carrier (AGC), continuing the shuttle to provide energy and enhance the body's oxidative phosphorylation and energy metabolism.[29] It's reported that Malate Ringer's fluid reduced myocardial injury in septic rats by improving mitochondrial function and inhibiting apoptosis, with L-malate playing a crucial role.[13] Our TPP@PAMAM encapsulating L-malate to form RPP@PAMAM@MA was confirmed in preliminary studies to target myocardial mitochondria, reducing consumption and delivering more L-malate to myocardial mitochondria, providing more raw materials for ATP synthesis.

Ferroptosis was a form of regulated cell death, closely associated with the production of mitochondrial lipid reactive oxygen species (ROS) and the destruction of the antioxidant system. Jang et al[30] found that mitochondria were involved in the onset of ferroptosis, since mitochondrial fragmentation and lipid peroxidation occurred shortly after ferroptosis-related stimuli, leading to inhibition of oxidative phosphorylation and electron transport chain (ETC) complexes, and therefore exacerbating RSL3-induced ferroptosis. Ye et al[31] discovered that inhibiting the ferroptosis SLC7A11/GPX4 pathway contributed to attenuating mitochondrial damage in the myocardium. Im et al[32] found that COX-2 functions as a cellular factor which induces superoxide-mediated cell death in primary cortical neurons. Cortical neurons with enhanced COX-2 expression showed superoxide generation, GSH depletion, and lipid peroxidation in response to low doses of Fe^{2+}. We also found substantial increases in MDA, GSSG, and Fe^{2+}, but decreases in GPX4 and GSH levels in cardiac tissues after hemorrhagic shock, indicating impaired antioxidant capacity, accumulation of lipid peroxides, and comprehensive disruption of redox homeostasis happened in the hemorrhagic shock-induced rat model. TPP-MR directly reduced mitochondrial ROS levels in myocardial cells, enhanced myocardial mitochondrial energy supply, and improved mitochondrial function. Furthermore, after TPP-MR infusion, the antioxidant capacity improved as the expression of GSH and GPX4 increase, but the expression of ACSL4 and COX2 decreased. By this way, TPP-MR infusion increased MAP and cardiac output, improved myocardial tissue perfusion, and significantly improved survival. Therefore, we hypothesized TPP-MR improved cardiac function in rats with hemorrhagic shock by reducing mitochondrial ROS and improving mitochondrial function via inhibiting ferroptosis.

Although this study observed the protective effects of TPP-MR on myocardial injury in hemorrhagic shock, whether it could protect patients with hemorrhagic shock remained to be further studied. What's more, the impact of extensive infusion of this fluid on the long-term prognosis of hemorrhagic shock also need further confirmation.

Conclusion

TPP-MR alleviated myocardial injury in rats with hemorrhagic shock by improving mitochondrial function and inhibiting ferroptosis.

Abbreviations

LR, Ringer's solution; MR, Malate Ringer's solution; HS, Hemorrhagic shock; MAP, mean arterial blood pressure; DA, dopamine; CO, cardiac output; HR, heart rate; CI, cardiac index; SI, stroke index; Bb, hemoglobin; cTnT, cardiac troponin T; LDH, lactate dehydrogenase; OMC, Oxoglutarate Malate carrier; AGC, aspartate glutamate carrier; MDA, malondialdehyde; ATP, Adenosine-triphosphate; VDAC2, voltage-dependent anion channel 2; GPX4, Glutathione peroxidase 4; TPP, Triphenyl phosphine; ACSL4, Acyl CoA Synthase Long Chain Family Member 4; NSH, N-monohydroxy succinimide; PAMAM, polyamidoamine; ANOVA, One-way analysis of variance.

Data Sharing Statement

The raw data of this study are available from the corresponding author on reasonable request.

Ethics Approval and Consent to Participate

The ethics and the protocols for the animal experiments were approved by the Ethical Committee of Army Medical University.

Author Contributions

All authors made a significant contribution to the work reported, whether that is in the conception, study design, execution, acquisition of data, analysis and interpretation, or in all these areas; took part in drafting, revising or critically reviewing the article; gave final approval of the version to be published; have agreed on the journal to which the article has been submitted; and agree to be accountable for all aspects of the work.

Funding

This study was supported by the National Natural Science Foundation of China (No. 82300561 and No. 82270523), The Chongqing Medical Young Talents Program, Natural Science Foundation of Chongqing (No. 2023NSCQ-MSX2877) and General Program of Joint Medical Research of Chong-qing Science and Health Commission and Chongqing Health Commission (2023MSXM127).

Disclosure

The authors report no conflicts of interest in this work.

References

1. Moore HB, Moore EE, Chapman MP, et al. Plasma-first resuscitation to treat hemorrhagic shock during emergency ground transportation in an urban area: a randomised trial. *Lancet*. 2018;392(10144):283–291. doi:10.1016/S0140-6736(18)31553-8
2. Cannon JW. Hemorrhagic Shock. *N Engl J Med*. 2018;378(4):370–379. doi:10.1056/NEJMra1705649
3. Ahmad FB, Anderson RN. The leading causes of death in the US for 2020. *JAMA*. 2021;325(18):1829–1830. doi:10.1001/jama.2021.5469
4. She H, Tan L, Zhou YQ, et al. The landscape of featured metabolism-related genes and imbalanced immune cell subsets in sepsis. *Front Genet*. 2022;21(13):821275. doi:10.3389/fgene.2022.821275
5. She H, Tan L, Wang Y, et al. Integrative single-cell RNA sequencing and metabolomics decipher the imbalanced lipid metabolism in maladaptive immune responses during sepsis. *Front Immunol*. 2023;27(14):1181697. doi:10.3389/fimmu.2023.1181697
6. Huen SC, Wang A, Feola K, et al. Hepatic FGF21 preserves thermoregulation and cardiovascular function during bacterial inflammation. *J Exp Med*. 2021;218(10):e20202151. doi:10.1084/jem.20202151
7. Fei QQ, Shalosky EM, Barnes R, et al. Macrophage-targeted lipid nanoparticle delivery of microRNA-146a to mitigate hemorrhagic shock-induced acute respiratory distress syndrome. *ACS Nano*. 2023;17(17):16539–16552. doi:10.1021/acsnano.3c01814
8. Evans L, Rhodes A, Alhazzani W, et al. Surviving sepsis campaign: international guidelines for management of sepsis and septic shock 2021. *Crit Care Med*. 2021;49(11):e1063–e1143. doi:10.1097/CCM.0000000000005337
9. Pérez-Liébana I, Juaristi I, González-Sánchez P, et al. A Ca2+ -dependent mechanism boosting glycolysis and OXPHOS by activating aralar-malate-aspartate shuttle, upon neuronal stimulation. *J Neurosci*. 2022;42(19):3879–3895. doi:10.1523/JNEUROSCI

10. Woodman OL, Long R, Pons S, et al. The cardiopro tectant 3', 4'-dihydroxyflavonol inhibits opening of the mitochondrial permeability transition pore after myocardial ischemia and reperfusion in rats. *Pharmacol Res*. 2014;81:26–33. doi:10.1016/j.phrs.2014.01.004
11. Zusman BE, Dixon CE, Jha RM, et al. Choice of whole blood versus lactated ringer's resuscitation modifies the relationship between blood pressure target and functional outcome after traumatic brain injury plus hemorrhagic shock in mice. *J Neurotrauma*. 2021;38(20):2907–2917. doi:10.1089/neu.2021.0157
12. Wei GJ, Chen JH, Jing ZQ, et al. Glucose transporter 1 (GLUT1)-targeting and hypoxia-activated mitochondria-specific chemo-thermal therapy via a glycosylated poly (amido amine)/celastrol (PAMAM/Cel) complex. *J Colloid Interface Sci*. 2022;608(Pt 2):1355–1365. doi:10.1016/j.jcis.2021.10.129
13. Tan L, She H, Peng XY, et al. Effects of Malate Ringer's solution on myocardial injury in sepsis and enforcement effects of TPP@PAMAM-MR. *J Transl Med*. 2022;20(1):591. doi:10.1186/s12967-022-03811-y
14. Dixon SJ, Lemberg KM, Lamprecht MR, et al. Ferroptosis: an iron-dependent form of nonapoptotic cell death. *Cell*. 2012;149(5):1060–1072. doi:10.1016/j.cell.2012.03.042
15. Tang D, Chen X, Kang R, et al. Ferroptosis: molecular mechanisms and health implications. *Cell Res*. 2021;31(2):107–125. doi:10.1038/s41422-020-00441-1
16. She H, Tan L, Du YL, et al. VDAC2 malonylation participates in sepsis-induced myocardial dysfunction via mitochondrial-related ferroptosis. *Int J Biol Sci*. 2023;19(10):3143–3158. doi:10.7150/ijbs.84613
17. Zeng YC, Cao GD, Lin L, et al. Resveratrol attenuates sepsis-induced cardiomyopathy in rats through anti-ferroptosis via the Sirt1/Nrf2 pathway. *J Invest Surg*. 2023;36(1):2157521. doi:10.1080/08941939
18. Guo NK, She H, Tan L, et al. Nano parthenolide improves intestinal barrier function of sepsis by inhibiting apoptosis and ROS via 5-HTR2A. *Int J Nanomed*. 2023;11(18):693–709. doi:10.2147/IJN.S394544
19. Nikita MP, Patel D, Collotta E, et al. Inhibition of the JAK/STAT pathway with baricitinib reduces the multiple organ dysfunction caused by hemorrhagic shock in rats. *Ann Surg*. 2023;278(1):e137–e146. doi:10.1097/SLA.0000000000005571
20. Liu PF, Feng YT, Li HW, et al. Ferrostatin-1 alleviates lipopolysaccharide induced acute lung injury via inhibiting ferroptosis. *Cell Mol Biol Lett*. 2020;27(25):10. doi:10.1186/s11658-020-00205-0
21. Li Q, Han XN, Lan X, et al. Inhibition of neuronal ferroptosis protects hemorrhagic brain. *JCI Insight*. 2017;2(7):e90777. doi:10.1172/jci.insight.90777
22. Li JJ, Chen Q, He XH, et al. Dexmedetomidine attenuates lung apoptosis induced by renal ischemia-reperfusion injury through α2AR/PI3K/Akt pathway. *J Transl Med*. 2018;16(1):78. doi:10.1186/s12967-018-1455-1
23. Maier CL, Brohi K, Curry N, et al. Contemporary management of major haemorrhage in critical care. *Intensive Care Med*. 2024. doi:10.1007/s00134-023-07303-5
24. Waksman R, Pahuja M, Van DS, et al. Standardized definitions for cardiogenic shock research and mechanical circulatory support devices: scientific expert panel from the shock academic research consortium (SHARC). *Circulation*. 2023;148:1113–1126. doi:10.1161/CIRCULATIONAHA.123.064527
25. Yeela TB, Noam B, Aviv AS, et al. Metabolomic and microbiome profiling reveals personalized risk factors for coronary artery disease. *Nat Med*. 2022;28(2):295–302. doi:10.1038/s41591-022-01686-6
26. Yang S, Zhang TY, Ge YL, et al. Ferritinophagy mediated by oxidative stress driven mitochondrial damage is involved in the polystyrene nanoparticles-induced ferroptosis of lung injury. *ACS Nano*. 2023;17(24):24988–25004. doi:10.1021/acsnano.3c07255
27. Wang ZJ, Xu SG, Qiu ZL, et al. Effect of sodium bicarbonate Ringer's solution on lung injury in rats with traumatic hemorrhagic shock. *J Biochem Mol Toxicol*. 2024;38(1):e23608. doi:10.1002/jbt.23608
28. Zhao HL, Zhu Y, Zhang J, et al. The beneficial effect of HES on vascular permeability and its relationship with endothelial glycocalyx and intercellular junction after hemorrhagic shock. *Front Pharmacol*. 2020;11:597. doi:10.3389/fphar.2020.00597
29. Wang YH, Stancliffe E, Fowle-Grider R, et al. Saturation of the mitochondrial NADH shuttles drives aerobic glycolysis in proliferating cells. *Mol Cell*. 2022;82(17):3270–3283.e9. doi:10.1016/j.molcel.2022.07.007
30. Yang JW, Mo JJ, Dai JJ, et al. Cetuximab promotes RSL3-induced ferroptosis by suppressing the Nrf2/HO-1 signalling pathway in KRAS mutant colorectal cancer. *Cell Death Dis*. 2021;12(11):1079. doi:10.1038/s41419-021-04367-3
31. Ye HR, He SS, Du Y, et al. Involvement of CD44 and MAPK14-mediated ferroptosis in hemorrhagic shock. *Apoptosis*. 2023. doi:10.1007/s10495-023-01894-6
32. Im JY, Kim D, Paik SG, et al. Cyclooxygenase-2-dependent neuronal death proceeds via superoxide anion generation. *Free Radic Biol Med*. 2006;41(6):960–972. doi:10.1016/j.freeradbiomed